

EVOLUTIONARY CALCULATIONS OF PHASE SEPARATION IN CRYSTALLIZING WHITE DWARF STARS

M. H. MONTGOMERY,^{1,2} E. W. KLUMPE,¹ D. E. WINGET,¹ & M. A. WOOD³

Received 1998 October 23; accepted 1999 May 25

ABSTRACT

We present an exploration of the significance of Carbon/Oxygen phase separation in white dwarf stars in the context of self-consistent evolutionary calculations. Because phase separation can potentially increase the calculated ages of the oldest white dwarfs, it can affect the age of the Galactic disk as derived from the downturn in the white dwarf luminosity function. We find that the largest possible increase in ages due to phase separation is ~ 1.5 Gyr, with a most likely value of approximately 0.6 Gyr, depending on the parameters of our white dwarf models.

The most important factors influencing the size of this delay are the total stellar mass, the initial composition profile, and the phase diagram assumed for crystallization. We find a maximum age delay in models with masses of $\sim 0.6M_{\odot}$, which is near the peak in the observed white dwarf mass distribution. In addition, we note that the prescription which we have adopted for the mixing during crystallization provides an upper bound for the efficiency of this process, and hence a maximum for the age delays. More realistic treatments of the mixing process may reduce the size of the effect. We find that varying the opacities (via the metallicity) has little effect on the calculated age delays.

In the context of Galactic evolution, age estimates for the oldest Galactic globular clusters range from 11.5 to 16 Gyr, and depend on a variety of parameters. In addition, a 4 to 6 Gyr delay is expected between the formation of the globular clusters and that of the Galactic thin disk, while the observed white dwarf luminosity function gives an age estimate for the thin disk of $9.5^{+1.1}_{-0.8}$ Gyr, without including the effect of phase separation. Using the above numbers, we see that phase separation could add between 0 to 3 Gyr to the white dwarf ages and still be consistent with the overall picture of Galaxy formation. Our calculated maximum value of $\lesssim 1.5$ Gyr fits within these bounds, as does our best guess value of ~ 0.6 Gyr.

Subject headings: dense matter—equation of state—stars: evolution—white dwarfs

1. ASTROPHYSICAL CONTEXT

The phenomenon of phase separation and crystallization exists within the larger context of white dwarf cooling. Since the time of Mestel's original treatment (Mestel 1952), much work has been done, both to improve the input physics of the models and to make more complete observations of the white dwarf luminosity function (WDLF). In 1987, Winget et al. showed that the observed downturn in the WDLF could be understood in terms of a finite age for the Galactic disk, and that the WDLF could therefore in principle be used to determine an age for the local Galactic disk. Using the preliminary results from Liebert, Dahn, & Monet (1988, hereafter LDM) for the observed WDLF, they obtained an age for the local Galactic disk in the range 7–10 Gyr. Since then, Wood has made more detailed calculations using improved input physics, Galactic evolution models, and WD parameters to constrain this age even further Wood (1990, 1992, 1995). Historically, these developments were foreshadowed by Schwarzschild (1958), Schmidt (1959), and D'Antona & Mazzitelli (1978), all of whom considered white dwarf evolution in a Galactic context.

Two observational surveys within the last ten years stand out in their importance to the field. First, Liebert et al. (1988) produced a WDLF containing 43 cool field WD's, which was the largest such sample size up to that point in time. More recently, Oswalt et al. (1996) produced a WDLF of 50 cool WD's in wide binaries. Using the models of Wood, the LDM sample yields an age for the Galactic Disk of $\sim 7.5 \pm 1$ Gyr (Wood 1995), while

the Oswalt et al. (1996) sample gives an age of $9.5^{+1.1}_{-0.8}$ Gyr. Taking the error estimates at face value, these results differ by 2σ . Wood & Oswalt (1998) conducted Monte Carlo simulations and found that it is unlikely that both samples are consistent with the same parent population. Further investigation will be needed to resolve the cause of this discrepancy.

In addition to the uncertainties in the observed WDLF, the way we treat various physical processes in white dwarf interiors greatly affects the ages that we derive for them. After the prediction in the early 1960's that white dwarfs should undergo a phase transition and crystallize as they cool (Abrikosov 1960; Kirzhnits 1960; Salpeter 1961), Mestel & Ruderman (1967) and Van Horn (1968) estimated that the associated release of latent heat during this process would be large enough to delay the cooling of white dwarfs significantly. Lamb & Van Horn (1975) included this energy release as part of their evolutionary calculations of a $1 M_{\odot}$ pure carbon white dwarf.

Stevenson (1977) was the first to propose a phase separation model that might affect white dwarf cooling times by providing an additional source of energy analogous to the release of latent heat. This model had a carbon core with trace amounts of iron. In a later model, Stevenson (1980) suggested that a uniform mixture of carbon and oxygen would become chemically differentiated as a result of the crystallization process. Because such a redistribution of elements could lower the binding (non-thermal) energy of the star, the change in energy would be added to the thermal energy, and hence the luminosity, of the

¹McDonald Observatory and Department of Astronomy, The University of Texas, Austin, TX 78712 - USA.

²Institut für Astronomie, Universität Wien, Türkenschanzstraße 17, A-1180 Wien, Austria.

³Department of Physics and Space Sciences and SARA Observatory, Florida Institute of Technology, Melbourne, FL 32901-6988 USA

star. This would increase the time for a white dwarf to cool to a given luminosity, and would extend the apparent age of the Galactic disk as derived from the WDLF.

Estimates of the amount by which the age of the local Galactic disk might be extended have ranged from 0.5 Gyr to 6 Gyr (Mochkovitch 1983; Barrat, Hansen, & Mochkovitch 1988; García-Berro et al. 1988; Chabrier et al. 1993; Segretain & Chabrier 1993; Hernanz et al. 1994; Segretain et al. 1994; Isern et al. 1997; Salaris et al. 1997), although recent estimates have been on the smaller end of this range, e.g., Salaris et al. (1997) calculate a delay of ~ 1.0 Gyr. Most of this spread in calculated age delays comes from differences in the assumed phase diagram, although the assumed C/O profile also has a large effect.

In the context of Galactic evolution, age estimates for the oldest Galactic globular clusters range from 13–16 Gyr (Pont et al. 1998) to 11.5 ± 1.3 Gyr (Chaboyer et al. 1998), and depend on a variety of parameters. In addition, a 4 to 6 Gyr delay is expected between the formation of the globular clusters and that of the Galactic thin disk (e.g., Burkert, Truran, & Hensler 1992; Chiappini, Matteucci, & Gratton 1997), while the observed white dwarf luminosity function gives an age estimate for the thin disk of $9.5_{-0.8}^{+1.1}$ Gyr (Oswalt et al. 1996), without including the effect of phase separation. Using the above numbers, we see that phase separation could add anywhere from 0 to 3 Gyr to the white dwarf ages and still be consistent with the overall picture of Galaxy formation.

In this paper, we examine the sensitivity of this calculated age delay to the various physical assumptions by varying the initial C/O profile of the white dwarf models, their total mass, and their H and He surface layer masses. In addition, we examine the effect of using two different published phase diagrams for the phase separation process, that of Segretain & Chabrier (1993) and that of Ichimaru, Iyetomi, & Ogata (1988).

Our work improves upon previous calculations of the age delay in that we use self-consistent evolutionary models. In particular, our models use the modern OPAL opacities (Iglesias & Rogers 1993) instead of the older Cox-Stewart opacities, and we are able to treat self-consistently the age delay as a function of total stellar mass, instead of using a relation scaled by mass for the connection between the core temperature and the surface luminosity. Finally, we are able to examine surface layer masses suggested by more recent asteroseismological investigations (Clemens 1993).

2. THE PHYSICS OF PHASE SEPARATION

2.1. Chemical Redistribution

Our present physical picture for the phenomenon of phase separation in white dwarf stars is as follows. As a white dwarf cools, it eventually reaches a temperature when its central regions begin to crystallize. This occurs when the thermal energy of the ions becomes much smaller than the energy of the Coulomb interactions between neighboring ions. As a result, the ions settle into lattice sites and lose the ability to move freely in three dimensions.

If the white dwarf interior is initially a mixture of C and O, then recent calculations indicate that the solid which crystallizes will have a higher O content than the fluid from which it formed (Ichimaru et al. 1988; Segretain & Chabrier 1993). Thus the crystallizing region of the white dwarf becomes O-enhanced and the fluid layer overlying this region becomes C-enhanced. Since the C is slightly less dense than the O at a given

pressure, this C-enhanced fluid layer is mixed via a Rayleigh-Taylor instability (Mochkovitch 1983; Isern et al. 1997) with the layers above, and C is transported outward from the center. As the white dwarf continues to crystallize, the O-enhanced crystalline core also continues to grow, with the net result that O is transported inward in the white dwarf and C is transported outward. Thus, the chemical composition profile after significant crystallization has occurred is different from the profile before crystallization.

Just how different this profile is depends on the particular phase diagram which is adopted for the process. In a “spindle” diagram, the solid which forms always has an enhanced concentration of the higher charge element (in this case oxygen), and the temperature of crystallization of the mixture lies between that of the individual elements. An “azeotropic” diagram differs from this in that there is a range of concentrations for which crystallization takes place *below* the temperature of crystallization of either of the pure elements. This is somewhat analogous to the phenomenon of “supercooling.” Finally, a “eutectic” phase diagram is one in which there is a near total separation of the higher and lower charged ions upon crystallization, resulting in a segregation of the two chemical species.

Stevenson’s original phase diagram (Stevenson 1980) was a eutectic phase diagram with C and O being immiscible in the solid phase, with the result that a pure O core would be formed in the models during crystallization. Using a density functional approach, Barrat et al. (1988) calculated a phase diagram of spindle type. In this case, the solid which forms is a C/O alloy, but with the O content of the solid enhanced relative to that of the fluid out of which it formed.

This problem was revisited by Ichimaru et al. (1988). They found that Stevenson’s initial prediction of a eutectic phase diagram was an artifact of his use of the random-alloy mixing (RAM) model for the internal energies in the solid phase. By comparison with Monte Carlo simulations, they found that the linear mixing formula is more accurate for the solid phase. They then used density-functional theory to derive a phase diagram of azeotropic type, which is shown as the dashed line in Figure 1. This diagram is similar to the spindle diagram, with the exception that there is a range of compositions for which the crystallization temperature is less than the crystallization temperature for either of the pure compositions.

Most recently, Segretain & Chabrier (1993) used a density-functional approach to derive phase diagrams for arbitrary binary-ionic mixtures, as a function of Z_1/Z_2 , where Z_1 and Z_2 are the nuclear charges of the two chemical species. For C and O ($Z_1/Z_2 = 0.75$), they obtain a phase diagram of spindle type, which is shown as the solid line in Figure 1.

As shown in Figure 1, these diagrams of Ichimaru et al. and Segretain & Chabrier differ slightly in the composition changes during crystallization, as well as in the temperatures at which crystallization takes place. As a result, they produce different chemical composition profiles after crystallization and different age delays.

We mention that the validity of the azeotropic phase diagram of Ichimaru et al. (1988) has recently been called into question by DeWitt, Slattery, & Chabrier (1996). DeWitt et al. find that the azeotropic diagram of Ichimaru et al. results from their use of the fitting function of Ogata & Ichimaru (1987) for the energies of the pure phases. The slight inaccuracies in this fitting function lead to incorrect values of the free energy for the pure phase, which in turn leads to a spurious departure from the linear mixing rule in the liquid. With this proviso, we have elected

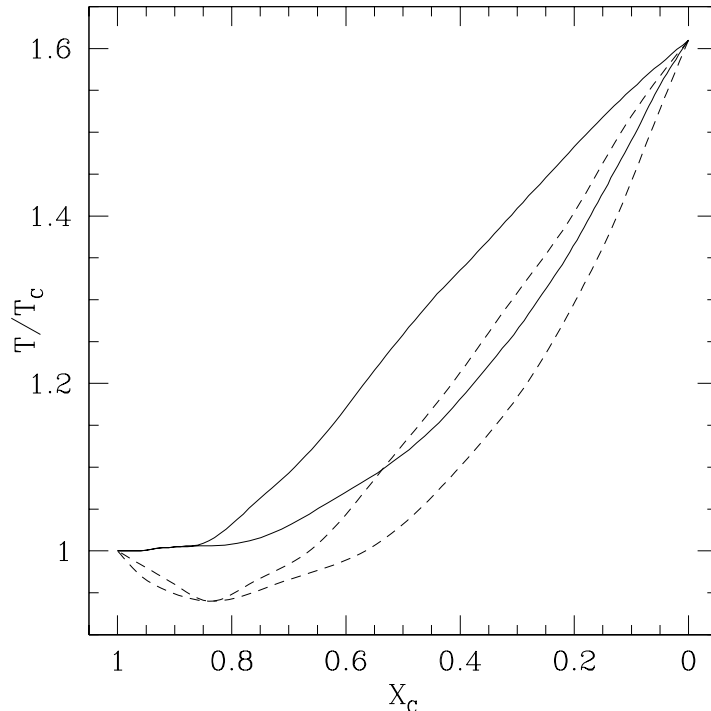


FIG. 1.— Phase diagrams for a C/O mixture as computed by Ichimaru et al. (1988, dashed line) and Segretain & Chabrier (1993, solid line), where the vertical axis is in units of the crystallization temperature of C, T_C , and the horizontal axis is the C mass-fraction. The solid line is of “spindle” type, while the dashed line is that of an “azeotrope.” The principal feature of the azeotrope is that there is a range of compositions for which the crystallization temperature of the mixture is less than that of either of the two constituents in the pure state.

to include calculations based on the phase diagram of Ichimaru et al. for purposes of comparison, in order to illustrate some of the uncertainties to which these calculations can be subject.

2.2. Energy Release

Because the distribution of C and O within a model changes during phase separation, the density profile changes as well. At a given pressure, O is slightly denser than C. A model which has undergone phase separation has more oxygen in its core, and thus a slightly larger concentration of mass in its central regions. As a result, the phase-separated model is more tightly bound gravitationally.

While it may be convenient to think of the energy which is released as being due solely to the change in the gravitational potential energy of the star, this is only part of the story. The relevant quantity is actually the total binding energy of the star, E_{bind} , which is the sum of all the nonthermal (structural) sources of energy. As such, it acts as a potential energy for the configuration. E_{bind} can be written as

$$E_{\text{bind}} = E_{\text{grav}} + E_{\text{deg}} + E_{\text{coul}} \quad (1)$$

where E_{grav} , E_{deg} , and E_{coul} are the respective energy contributions from gravitational interactions, kinetic energies of the degenerate electrons, and Coulomb interactions among the different charged particles (ions and electrons).

As phase separation occurs and the central regions become oxygen enriched, the central density of the model increases. Thus, E_{grav} becomes more negative, as does E_{coul} . E_{deg} , however, becomes more positive, since the Fermi energy of the electrons increases with increasing density. Summing these contributions, we find that there is a net decrease in E_{bind} for the models considered here. Due to conservation of energy, this energy

must be used to increase the thermal energy of the ions, which are the only significant repository of thermal energy in the cores of our white dwarf models. This energy, then, is available to be radiated away and acts as an additional luminosity source.

The various contributions to the photon luminosity L and the neutrino luminosity L_ν of the white dwarf may be formally written as (e.g., Isern et al. 1997; Chabrier 1998)

$$L + L_\nu = - \int_0^{M_{\text{WD}}} dm \left[C_v \frac{dT}{dt} + T \left(\frac{\partial P}{\partial T} \right)_{v, X_O} \frac{dV}{dt} + \left(\frac{\partial u}{\partial X_O} \right)_{T, V} \frac{dX_O}{dt} \right] \quad (2)$$

where $V = 1/\rho$ is the specific volume, X_O is the mass-fraction of the heavier of the two chemical species (in this case, oxygen), and u is the internal energy per unit mass, which contains thermal, electron degeneracy, and Coulomb contributions. The first term in the integrand on the righthand side of equation 2 is due to the heat capacity of the core, which includes the release of latent heat of crystallization, while the second term gives the contribution to the luminosity due to volume changes, and is usually small in white dwarfs since the pressure P is only a weak function of the temperature. The final term gives the luminosity due to the changing chemical composition profiles within the white dwarf. This is the term we will study in our numerical calculations.

As a check on the direct evolutionary calculations, we can estimate the age delay produced by a given energy release. If we denote by dE a small amount of energy which is released during the process of phase separation, and if we assume that this

energy is quickly radiated, then we can calculate an estimated age delay t_d :

$$t_d = \int \frac{dE}{L}. \quad (3)$$

In the context of a sequence of evolutionary models, this integral is operationally a sum, since a given model is computed at discrete points in time, luminosity, etc. Furthermore, since the energy ΔE_i is released *between* luminosities L_{i-1} and L_i , say, the average luminosity at which the energy is released is approximately $(L_{i-1} + L_i)/2$, so the discrete version of equation 3 becomes

$$t_d = \sum_i \frac{\Delta E_i}{\frac{1}{2}(L_{i-1} + L_i)}. \quad (4)$$

We have used equation 4 as an alternate prescription to calculate age delays. For the larger energy releases, t_d computed in this way agrees with the delay calculated from the self-consistent evolutionary calculations, and for small energy releases it provides a better estimate since the small energies can become masked in the numerical noise of the evolutionary calculations.

3. NUMERICS

The basis for these calculations is WDEC, the White Dwarf Evolutionary Code, as described in Lamb & Van Horn (1975), and in Wood (1990). Our current version uses the updated OPAL opacity tables (Iglesias & Rogers 1993; Wood 1993). We use the additive volume technique to treat the equation of state of the C/O mixture in the cores of our models.

3.1. The Melting Curve

Our criterion for crystallization is given by the phase diagram which we adopt, with the following caveat. Our equation of state (EOS) is based on the Lamb EOS code (Lamb & Van Horn 1975), which has $\Gamma \simeq 160$ at crystallization. Here, $\Gamma \equiv Z^2 e^2 / \langle r \rangle k_B T$ is the ratio of Coulomb energy between neighboring ions to each ion's kinetic energy. More recent calculations indicate that $\Gamma \simeq 180$ (Ogata & Ichimaru 1987). As a result, our values for the crystallization temperature of C, $T_{C,\text{xtal}}$, are too high by a factor of $\sim 180/160 = 1.125$.

To remedy this situation, we could simply adjust $T_{C,\text{xtal}}$ downward accordingly, and we have done this for a few runs. This is inconvenient, however, because it places us at the edge of our EOS tables which were calculated with $\Gamma \simeq 160$. Instead, we apply a correction factor to our calculated age delays which takes into account the fact that crystallization/phase separation occurs at lower central temperatures, and therefore lower luminosities, than is calculated directly in our models. This correction to the calculated age delays is typically of order 25%. For example, an age delay due to phase separation computed with $\Gamma \simeq 160$ might be ~ 1 Gyr, which with the more physical value of $\Gamma \simeq 180$ would be ~ 1.25 Gyr. We find that this procedure of computing the age delays based on the corrected luminosity during crystallization to be accurate to within 1–2%.

3.2. Implementation in WDEC

The calculation of the evolutionary sequences is “quasi-static” in the sense that we compute a sequence of static models separated by finite steps in time. Each static model represents the cooling white dwarf at a different age and luminosity. We include the physics of phase separation using the same approximation: we assume that the timescale for any mixing which occurs is short compared to the individual evolutionary timesteps

(see section 3.3 of this paper; Mochkovitch 1983; Isern et al. 1997), and we assume that the binding energy which is released by this process can be modeled by some suitably chosen local energy generation rate, ϵ_{ps} (e.g., Isern et al. 1997).

The phase separation calculation may therefore be broken into three sections. The first part involves obtaining the changing composition profile as a function of the crystallized mass-fraction, while the second part is the calculation of the cumulative energy released, also as a function of the crystallized mass-fraction. The final part is the calculation of the value of ϵ_{ps} , which is the energy locally deposited per unit mass per unit time. Our implementation of the complete problem is self-consistent in that we let ϵ_{ps} vary as the compositional profile changes due to crystallization, as WDEC iterates to a converged model.

The first part of the overall problem relates to the composition of the crystallizing layers. Using the phase diagram of Segretain & Chabrier (1993) or Ichimaru et al. (1988), we compute the final composition profile of the model given the initial profile, before doing a full evolutionary calculation. This is possible because the composition of the crystals which are forming is determined solely by the mass fractions of C and O which are present in the fluid phase, and not by the temperature and density of the medium (the temperature and density of course determine *when* the fluid crystallizes, but given that it is crystallizing, the chemical composition of the solid is determined *solely* by the composition of the fluid). We are therefore required to compute only once, at the onset of crystallization, the composition profile as a function of the crystallized mass fraction. At subsequent evolutionary times, we use this relation and the current crystallized mass-fraction to interpolate onto the composition grid, which is a computationally convenient procedure.

We take this same approach for the calculation of the energy released. At the onset of crystallization, we calculate the total amount of energy released as a function of M_{xtal}/M_* , using the relation

$$\delta E = \int_0^{M_{\text{wd}}} \left(\frac{\partial u}{\partial X_{\text{O}}} \right)_{T,V} \delta X_{\text{O}} dm, \quad (5)$$

where δE is the binding energy released by the composition change δX_{O} . Since these changes in composition are with respect to the pre-crystallization state, we are in effect holding both the temperature and density profiles constant for all subsequent phases of crystallization. Holding the temperature profile constant is a quite reasonable approximation, since the vast majority of the mass in the the white dwarf model is strongly degenerate for the temperature range of interest. Similarly, we expect the changes in the density profile to be small ($\frac{\delta \rho}{\rho} \lesssim 1\%$) even in the presence of composition changes. This is a consequence of the fact that the equations of state for carbon and oxygen are very similar in the strongly degenerate regime, i.e., μ_e , the atomic mass per electron, is 2.0 for both elements. This suggests that this approach would not necessarily be as accurate for carbon and iron, since $\mu_e = 2.15$ for iron.

Figure 2 provides the final justification for our assumptions. The filled dots represent the energy released as computed self-consistently at each evolutionary time step, and the solid line is the calculated energy released assuming a static density and temperature profile as described in the above paragraph. The best agreement is for smaller amounts of crystallization, since these models differ the least from the initial static model. Even near complete crystallization, however, the difference between

the two values is less than 0.5%, justifying our assumptions. Computationally, it is very convenient to compute the energy release just once at the outset and then interpolate using the present value of the crystallized mass fraction. This allows WDEC to avoid doing a calculation of the energy release for each iteration of each model, which would significantly affect the speed of the calculations.

Because all our calculations are done on evolutionary timescales, we do not have any information about the actual dissipative processes which are responsible for depositing the energy of phase separation locally. Indeed, without an accurate hydrodynamic model of the mixing process, this is not possible. Fortunately, it is more important to know the total energy released rather than exactly how this energy is deposited within the white dwarf model. This is because the core has a very high thermal conductivity, which tends to smooth out the temperature distribution. Thus, wherever the energy is initially deposited, it will soon be shared throughout the core; indeed, an isothermal core was an assumption of the original Mestel theory (1952), and it is still a very accurate description of the physics in the interiors of white dwarfs (e.g., García-Berro et al. 1996; Segretain et al. 1994). We therefore choose ϵ_{ps} such that the local temperature is increased by the same fractional amount throughout the core, i.e., $\frac{\delta T}{T} = \text{const.}$, while we simultaneously require that the total energy deposited in this way is equal to the energy released due to phase separation in a given timestep. This is somewhat analogous to the analytical approach outlined by Isern et al. (1997), although we developed our approach for ease of numerical implementation.

There is one final adjustment which we make to the value of ϵ_{ps} as calculated above. It is due to the fact that WDEC calculates models quasi-statically, so that ϵ_{ps} is assumed to have been constant during the last time step taken, when in fact it may have changed by a substantial amount. Put another way, the value of ϵ_{ps} which WDEC calculates should be associated with the average luminosity of the present and previous timesteps, not just the current luminosity. Thus, WDEC is implicitly calculating a delay based upon

$$t_d = \sum_i \frac{\Delta E_i}{L_i} \quad (6)$$

instead of the expression in equation 4. We can remedy this situation by an appropriate rescaling of ϵ_{ps} . If we rescale ΔE_i , and hence ϵ_{ps} , by $2L_i/(L_i + L_{i-1})$, then equation 6 is transformed into equation 4, and we recover the correct age delay due to crystallization when implemented in the evolution code. In the limit that our timesteps are very small, the above prescription is not necessary, but such small timesteps would be computationally inconvenient, both from a cpu-time standpoint and from a numerical convergence standpoint.

3.3. Consistency Checks

We use three different initial C/O profiles in our analysis. In Figure 3 we show the oxygen composition in the core both before (dotted line) and after (solid line) crystallization has taken place. We have taken a homogeneous 50:50 C/O initial distribution and assumed complete mixing of the overlying fluid layers as crystallization takes place. This should place an upper limit on the effect which phase separation can have on any particular model. We note that the composition profile after crystallization assuming the Segretain & Chabrier (1993) phase diagram agrees well with that given in Chabrier et al. (1993).

Figure 4 shows a different initial oxygen profile which is computed in Salaris et al. (1997) for a $0.61 M_\odot$ white dwarf model. This profile was obtained by considering nuclear reaction processes in the white dwarf progenitor. Here we use a modified algorithm for mixing which reduces to the ‘‘complete mixing’’ algorithm when applied to an initially flat distribution. When a shell crystallizes, we check to see if the enhanced carbon content of the innermost fluid shell now has more carbon than the shell overlying it. If it does, then we mix the two shells and perform the same comparison with the next shell farther out, mixing all three shells if necessary. In this way, we move outward through the fluid until further mixing no longer decreases the carbon content of the fluid between this point and the crystallization boundary. This is physically reasonable, since carbon is, in this sense, ‘‘lighter’’ than oxygen, so these layers should be mixed by a convective instability.

For completeness, we use a third profile taken from Wood (1990) and Wood (1995). It is designed to be representative of C/O profiles calculated in Mazzitelli & D’Antona (1986) and D’Antona & Mazzitelli (1989), who also consider nuclear reaction rates. Algebraically, it is given by

$$X_{ox} = \begin{cases} 0.75 & 0.0 \leq q \leq 0.5 \\ 0.75 - 1.875(q - 0.5) & 0.5 < q \leq 0.9 \\ 0.0 & 0.9 < q \leq 1.0 \end{cases} \quad (7)$$

where $q = M_r/M_*$ and $X_c = 1 - X_{ox}$.

Our treatment of the mixing process provides an upper bound for the efficiency of this process. If we were to perform a more self-consistent calculation, we would compute the Brunt-Väisälä frequency for a given chemical composition profile in the model and mix those layers which were convectively unstable *and* whose computed timescales for mixing were shorter than the individual timesteps in our evolutionary calculations. An analytical approach to this more detailed problem is given in Isern et al. (1997) and Mochkovitch (1983). Here we merely note that a typical value of $|N^2|$ for a Rayleigh-Taylor unstable region in the cores of our models is $\sim 10^{-4}$, yielding a timescale for the mixing instability of $\frac{1}{|N|} \sim 10^2$ s, which is clearly shorter than the relevant timescales for evolution.

4. A SIMPLE TEST PROBLEM

As a check of the standard approach to treating phase separation, we performed a simplified treatment of that given in Xu & Van Horn (1992), in which they calculate the change in binding energy of a zero-temperature C/Fe white dwarf which undergoes phase separation. In order to do this, we have written a separate code which implements the equations for a zero-temperature degenerate electron gas. Our approach is simpler in that we do not include Coulomb effects in our EOS calculations, so our approach is essentially pure Chandrasekhar theory (Chandrasekhar 1939). We do include, however, relativistic effects, which Xu & Van Horn are unable to treat. In testing this approach to phase separation, we compute the energy released due to phase separation in two different ways. First, we directly compute the global change in the binding energy. Second, we use the expression for the local energy release and integrate this over the mass of the model, as given in equation 5. To further simplify things, we have taken the initial state to be one in which the distribution of Fe and C is uniform throughout the model, and we have taken the final state to be a pure Fe core surrounded by a pure C mantle.

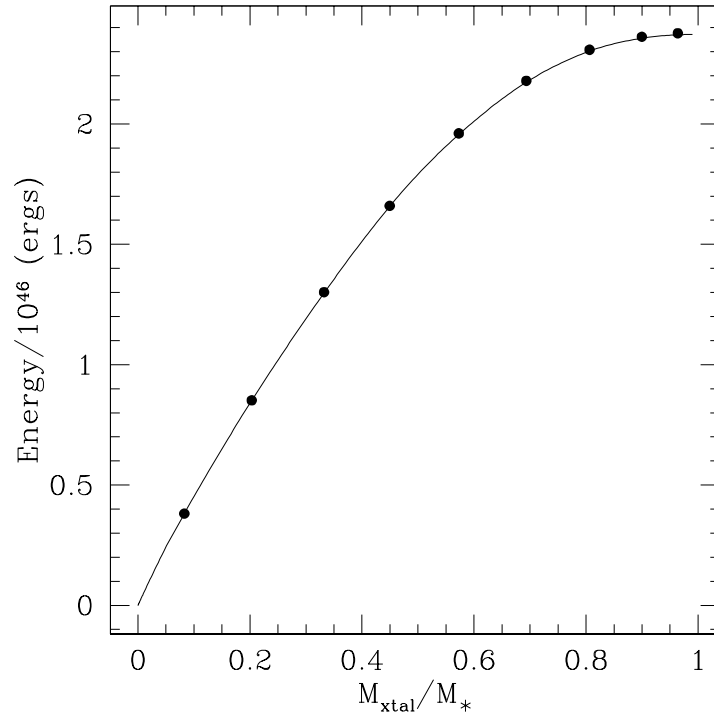


FIG. 2.— A comparison of the energy released during crystallization from a static calculation (line) with that from a self-consistent evolutionary calculation (filled dots). The error for the total energy released at complete crystallization is less than 0.5%.

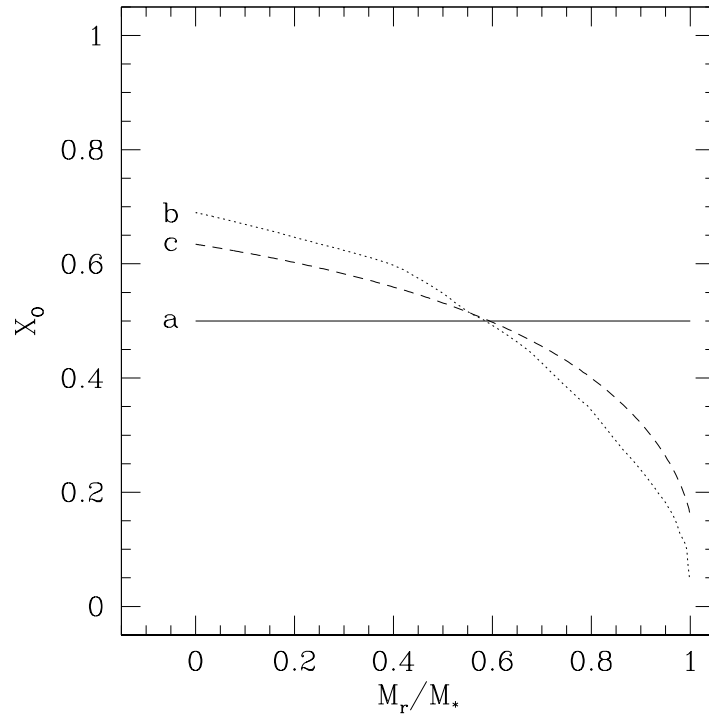


FIG. 3.— Before crystallization has occurred, we have assumed a 50:50 C/O mixture, as shown by the solid line (a). After crystallization is complete, the oxygen profile is given by the dotted line (b) if the phase diagram of Segretain & Chabrier (1993) is used, and by the dashed line (c) if the phase diagram of Ichimaru et al. (1988) is used. We have assumed complete mixing of the remaining fluid layers at each stage of crystallization. It is the redistribution of matter from the initial to the final profile which results in a net decrease in the overall binding energy of the configuration. This model is for a $0.6 M_{\odot}$ white dwarf.

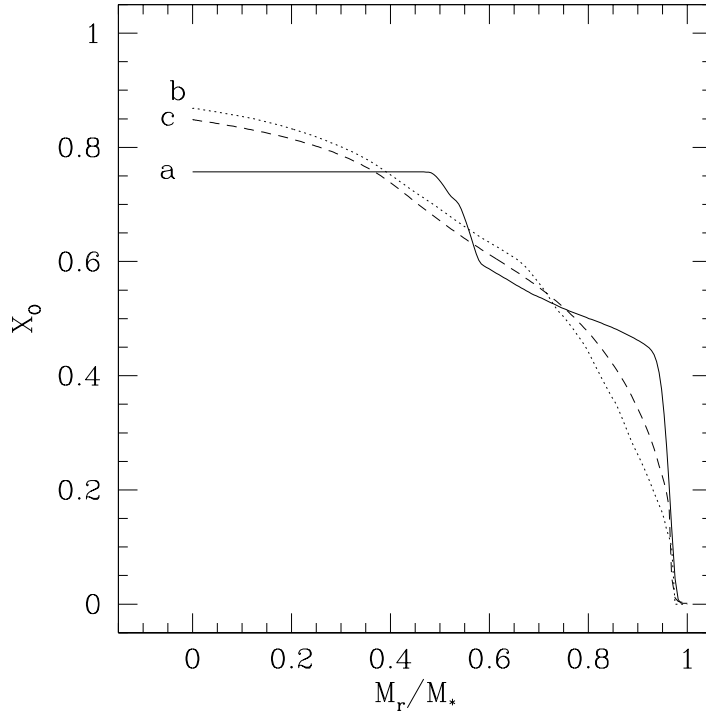


FIG. 4.— The same as Figure 3, except that the initial C/O profile (a) is that computed by Salaris et al. (1997) for a $0.61 M_{\odot}$ white dwarf model. Curves (b) and (c) are the final profiles assuming the Segretain & Chabrier (1993) and Ichimaru et al. (1988) phase diagrams, respectively. Note that the oxygen mass-fraction at the very center increases by only about 15% during crystallization in this case, as compared with a 40% increase for the central value in Figure 3. Thus, less energy is liberated.

Figure 5 shows the results for differing initial fractions of C and Fe. For instance, for an initial 50:50 C/Fe distribution we calculate an energy release of about $1.9 \cdot 10^{48}$ ergs, with less than a 5% relative error between the two methods. Even this small amount of error decreases as we approach a pure Fe or C initial state. This is because the density and composition changes before and after phase separation are now smaller, which makes the local calculation more accurate. For instance, if the model is 99% C uniformly distributed initially, then after phase separation most of it (99% in fact) is pure C. The contrast between 99% and 100% is small enough that the local density and composition changes are also small ($\delta X_C \lesssim 1\%$, $\frac{\delta \rho}{\rho} \lesssim 0.1\%$), which means that the approximation involved in making the infinitesimal variations in equation 5 finite is more accurate. We note that it is possible to perform such a simplified treatment for a C/Fe white dwarf model and still obtain meaningful results, while for a C/O model it would not be possible. This is because $\mu_e = 2.0$ for both C and O, while $\mu_e = 2.15$ for Fe. Thus, ignoring Coulomb effects, C and O have identical equations of state, while C and Fe are still nontrivially different in this approximation.

The results of this test problem (Figure 5) convince us that by applying equation 5, we are correctly calculating the change in the binding energy of the configuration, and thus the amount of thermal energy which has been liberated from structural sources. This shows us that the overall approach to this problem which we use here, and which has been used in the past, is sound and accurately describes the physics of phase separation.

5. RESULTS

5.1. $0.6 M_{\odot}$ White Dwarf Models

In Table 1 we give an evolutionary listing of our fiducial sequence (other sequences are available from the author upon request). This sequence is more than just a convenient reference model for the rest of our calculations. Given the observed peak of the masses of isolated white dwarfs in the vicinity of $0.6 M_{\odot}$ (Weidemann & Koester 1983; Weidemann & Yuan 1989; Bergeron et al. 1995; Lamontagne et al. 1997), this model will be the most useful in our comparisons with the white dwarf population as a whole. For the surface layer masses, we have taken $M_{\text{He}}/M_* = 10^{-2}$ and $M_{\text{H}}/M_* = 10^{-4}$ as in Wood (1995). We explore the effect of different surface layer masses later in this section.

We now wish to consider the effect of phase separation on actual evolutionary sequences. We compute this effect in two different ways. Using the first method, we compare sequences in which the physics of phase separation is included with those in which it is not. Taking two such sequences, we first perform a spline fit for each sequence's age over a fixed luminosity grid, and then we calculate the difference in ages at each luminosity. The results are given by the solid line in Figure 6, and indicate an age delay at complete crystallization of about 1.5 Gyr; this is for an initially homogeneous 50:50 C/O profile with an assumed metallicity of $Z = 0.000$ in the opacities. We note that all the age delays computed here are for complete crystallization of our models, and hence represent upper limits to the possible age delays. Operationally, our models are almost completely crystallized near the observed luminosity turndown at $\log L_*/L_{\odot} \sim -4.5$, so that there is at most a 1% change in our calculated age delays if we only consider models which have not yet cooled beyond this point.

The other method involves applying equation 4 to a sequence undergoing phase separation, which is shown by the dotted line

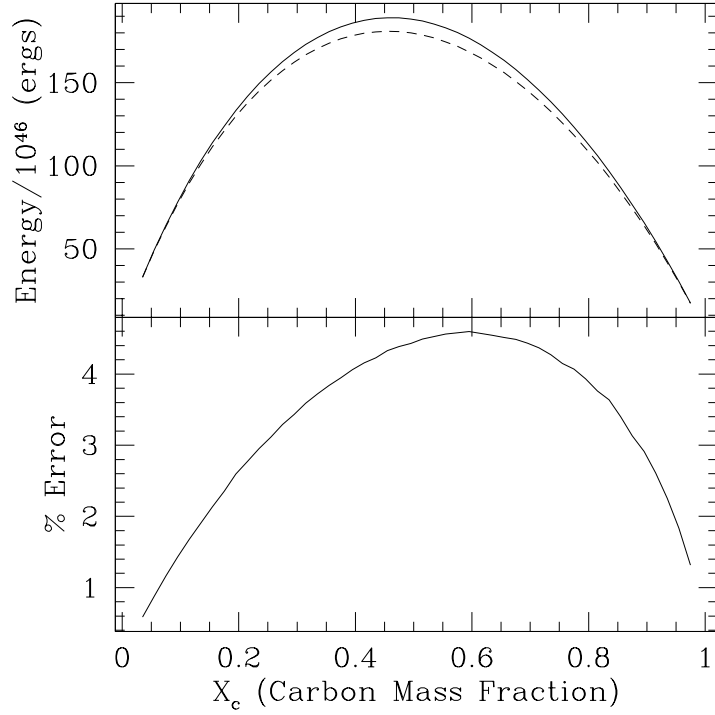


FIG. 5.— The upper panel shows the energy released due to phase separation as a function of X_c , the carbon mass-fraction. The model is a C/Fe mixture computed assuming pure Chandrasekhar theory. The solid line comes from a direct calculation of the change in binding energy, and the dotted line is obtained from the application of equation 5. The lower panel shows the percent error between these two methods. The total mass of the model is set to $0.66546 M_\odot$, as in Xu & Van Horn (1992).

TABLE 1
FIDUCIAL WHITE DWARF COOLING SEQUENCE WITHOUT PHASE SEPARATION

$\log L/L_\odot$	$\log \text{Age (yr)}$	$\log T_c$	$\log T_{\text{eff}}$	$\log R_\star$	$\log L_\nu/L_\odot$	M_{xtal}/M_\star
1.0000	5.917	7.950	4.869	9.131	1.298	0.000
0.6000	6.158	7.891	4.793	9.084	0.946	0.000
0.2000	6.376	7.843	4.710	9.049	0.581	0.000
-0.2000	6.592	7.798	4.623	9.024	0.193	0.000
-0.6000	6.855	7.737	4.533	9.004	-0.230	0.000
-1.0000	7.204	7.660	4.440	8.989	-0.886	0.000
-1.2000	7.429	7.604	4.394	8.982	-1.356	0.000
-1.4000	7.674	7.531	4.346	8.976	-1.956	0.000
-1.6000	7.903	7.448	4.299	8.971	-2.670	0.000
-1.8000	8.097	7.360	4.251	8.967	-3.449	0.000
-2.0000	8.264	7.273	4.203	8.963	-4.248	0.000
-2.2000	8.413	7.187	4.155	8.959	-5.042	0.000
-2.4000	8.550	7.103	4.106	8.956	-5.804	0.000
-2.6000	8.679	7.021	4.058	8.953	-7.279	0.000
-2.8000	8.805	6.940	4.009	8.951	< -10.00	0.000
-3.0000	8.930	6.860	3.961	8.948	< -10.00	0.000
-3.2000	9.055	6.778	3.912	8.946	< -10.00	0.000
-3.4000	9.182	6.694	3.863	8.944	< -10.00	0.000
-3.6000	9.317	6.613	3.814	8.942	< -10.00	0.059
-3.8000	9.497	6.518	3.765	8.939	< -10.00	0.379
-4.0000	9.704	6.350	3.717	8.935	< -10.00	0.804
-4.2000	9.825	6.176	3.668	8.933	< -10.00	0.961
-4.4000	9.900	6.022	3.618	8.933	< -10.00	0.989
-4.6000	9.953	5.891	3.569	8.932	< -10.00	0.990

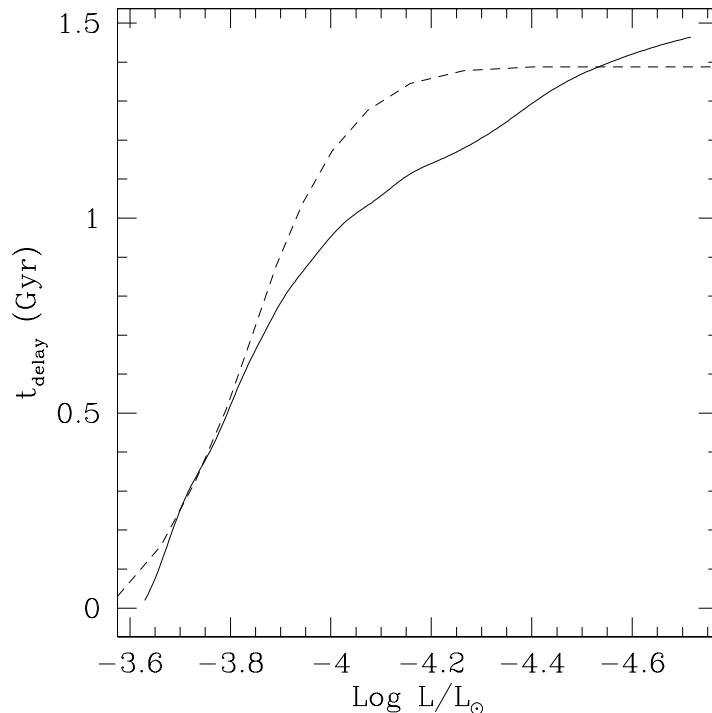


FIG. 6.— The solid line is a self-consistent calculation of the age difference between two $0.6 M_{\odot}$ white dwarf evolutionary sequences with $Z = 0.0$, one of which is undergoing phase separation. The dotted line is the result of applying equation 4 to the evolutionary sequence undergoing phase separation, which yields an asymptotic value for the age delay of ~ 1.4 Gyr. At complete crystallization ($\log L/L_{\odot} \sim -4.6$), the value given by the direct evolutionary calculation is within 5% of this, indicating that the basic physics which is operating is well-described by equation 3.

in Figure 6. This yields an asymptotic value for the age delay of 1.38 Gyr, which is within 5% of the age difference computed with the first method. This result indicates that the basic physics which is operating is well-described by equation 4, i.e., the energy being released by phase separation is mostly being radiated in a given timestep. For the remainder of the results quoted here, the age delays have been calculated using this second method (equation 4), since this proves to be more accurate for the cases involving smaller energy releases and age delays.

We now study the effect of the initial composition profile on the age delays. We use three different profiles: one which is a homogeneous 50:50 mix (Figure 3), one calculated by Salaris et al. (1997) (Figure 4), and one given by equation 7. Our results are summarized in Table 2, where the columns labeled SC and IIO indicate that we have used the phase diagrams of Segretain & Chabrier (1993) and Ichimaru et al. (1988), respectively. Near the centers of these models, we found that the initial/final oxygen mass-fraction changed by only about 15% in the initially stratified case in Figure 4, as compared to 40% in the homogeneous case in Figure 3. Because less matter is being redistributed in the initially stratified case, we would expect less energy to be released as a result. Using the phase diagram of Segretain & Chabrier (1993) applied to a $0.6 M_{\odot}$ white dwarf model, we find that in the homogeneous case $2.38 \cdot 10^{46}$ ergs are released whereas in the initially stratified case in Figure 4 only $1.03 \cdot 10^{46}$ ergs are released. These energies result in age delays of 1.38 Gyr and 0.62 Gyr, respectively. Thus, the initial composition profile has a large effect on the calculated age delays. In addition, the Ichimaru et al. (1988) phase diagram produces smaller composition changes and hence smaller values, reducing the Segretain & Chabrier age delays by approximately one-third.

We now consider the effect of a nonzero metallicity in the opacity tables. The effect of varying the metallicity from $Z = 0.000$ to $Z = 0.001$ results in a change of less than 0.016% in the energies released, and is barely detectable numerically. The main effect of changing the metallicity is to affect the luminosity range at which the phase separation energy is released, which in turn affects the age delay, t_{delay} . For both the homogeneous and stratified case, the average luminosity during crystallization changes by less than 3% as Z is varied from 0.000 to 0.001, and hence t_{delay} also changes by less than 3%. Thus, the age delay is essentially insensitive to the metallicity assumed for the opacities.

Finally, we summarize the effect of different surface layer masses in Table 3. For $M_{\text{He}}/M_{\star} = 10^{-3}$ and $M_{\text{H}}/M_{\star} = 10^{-5}$ (comp1), we find maximum age delays of 1.45 Gyr, and for $M_{\text{He}}/M_{\star} = 10^{-4}$ and $M_{\text{H}}/M_{\star} = 10^{-6}$ (comp2), our maximum calculated age delay is 1.56 Gyr. These values represent increases of 5% and 13%, respectively, over the age delays calculated in our fiducial model. For clarity, we note that these calculations are for the age differences introduced by phase separation alone at these new surface layer masses; the white dwarf ages themselves change significantly with He layer mass, which produces a decrease in the calculated ages (without including phase separation) of ~ 0.75 Gyr for each order of magnitude increase in M_{He} . Again, we find that varying the metallicity in the opacities has a small effect on these numbers, at only the 1% level.

5.2. The Mass Dependence

The mass of the white dwarf model affects the process of phase separation in two main ways, as is illustrated in Figure 7. First, a more massive white dwarf has a higher gravity so that more energy is released by the subsequent rearrangement

TABLE 2
AGE DELAYS FOR $0.6M_{\odot}$ MODELS

Initial Profile	Delay (Gyr)	
	SC	IIO
50:50 homogeneous	1.38	0.99
stratified (Salaris et al. 1997)	0.62	0.39
stratified (Wood 1995)	0.30	0.20

TABLE 3
AGE DELAYS FOR $0.6M_{\odot}$ MODELS WITH DIFFERENT SURFACE LAYER MASSES

Initial Profile	Delay (Gyr)				
	comp1		comp2		
	SC	IIO	SC	IIO	IIO
50:50 homogeneous	1.45	1.04	1.56	1.12	1.12
stratified (Salaris et al. 1997)	0.66	0.42	0.71	0.44	0.44
stratified (Wood 1995)	0.32	0.21	0.34	0.23	0.23

of matter. Second, the luminosity at which crystallization occurs is higher for a more massive white dwarf, which tends to lessen the age-delay for a given energy release. For example, even though the total energy released in a $1.2 M_{\odot}$ model increases by a factor of ~ 10 , the average luminosity increases by a factor of ~ 30 , and hence there is a net decrease in the time delay relative to the $0.6 M_{\odot}$ sequence.

The competition of these two effects suggests that there may be a mass for which there is a maximum age-delay, for a fixed composition profile. This is indeed the case, as is demonstrated in Figure 8. We find that the $0.6 M_{\odot}$ white dwarf models have the maximum age-delays for a given composition profile (this was also found by Segretain et al. 1994). The calculated age delay is only weakly dependent upon the metallicity, as can be seen from the small difference between the solid and dashed curves. It is strongly dependent upon the initial profile, however, which can decrease the energy release, and hence the age-delays, by a factor of three or more, as is shown in Figure 8.

From the preceding calculations we find that the two most important factors influencing the magnitude of the age delays introduced by the physics of phase separation are the *mass* of the white dwarf model and its *initial C/O* profile. Because the mass range of observed white dwarfs is strongly peaked around $0.6M_{\odot}$ (e.g., Lamontagne et al. 1997), we find that the age delay we calculate is near the maximum possible with respect to this parameter. In terms of the initial C/O profile, however, the situation is reversed. For a $0.61M_{\odot}$ white dwarf model, the profile calculated by Salaris et al. (1997) reduces the age delay by a factor of ~ 2 from the 50:50 homogeneous case. Using the profile of Wood (1995), which is based on results from Mazzitelli & D’Antona (1986) and D’Antona & Mazzitelli (1989), the reduction factor is ~ 5 .

If we take as our best guess the initial profile of Salaris et al. (1997), assume a $0.6M_{\odot}$ white dwarf model with $M_{\text{He}}/M_{\star} = 10^{-2}$ and $M_{\text{H}}/M_{\star} = 10^{-4}$, and use the Segretain & Chabrier (1993) phase diagram, then we obtain an age delay of ~ 0.6

Gyr.

6. CONCLUSIONS

We find a maximum age delay of ~ 1.5 Gyr due to phase separation for our fiducial white dwarf model ($M_{\star} = 0.6M_{\odot}$) and a best guess age delay of ~ 0.6 Gyr. Salaris et al. (1997) have recently calculated a value of ~ 1 Gyr, using the evolutionary models of Wood & Winget (1989). If we scale their value to our present models (assuming an average luminosity during crystallization for their models of $\log L/L_{\odot} \simeq -4.1$), then we obtain 0.75 Gyr, which is in basic agreement with our estimate of 0.62 Gyr. The differences in these models are mainly due to the different surface layer masses adopted; more recent asteroseismological analyses of the class of DA’s suggests that the appropriate surface layer masses are $M_{\text{He}}/M_{\star} \sim 10^{-2}$ and $M_{\text{H}}/M_{\star} \sim 10^{-4}$ (Clemens 1993, 1995), and these are the values which we have assumed.

The most important factors influencing the size of the calculated age delay are the total stellar mass and the initial composition profile. We find the largest age delays occur in models with masses of $\sim 0.6M_{\odot}$, near the peak in the observed white dwarf mass distribution. The best current theoretical initial C/O profile produces models with smaller age delays, of ~ 0.6 Gyr. In addition, if we use the phase diagram of Ichimaru et al. (1988) instead of the Segretain & Chabrier (1993) phase diagram, then our age delays are reduced by about one-third. We note that the prescription which we have adopted for the mixing during crystallization provides an upper bound for the efficiency of this process, and hence a maximum for the age delay. More realistic treatments of the mixing process may reduce the age delay. We find that varying the opacities (via the metallicity) and varying the surface layer masses has only a small effect ($\lesssim 10\%$) on the calculated age delays.

Our calculations do not take into account the possible age delays introduced by the phase separation of heavier trace-element species such as ^{22}Ne , which may produce significant

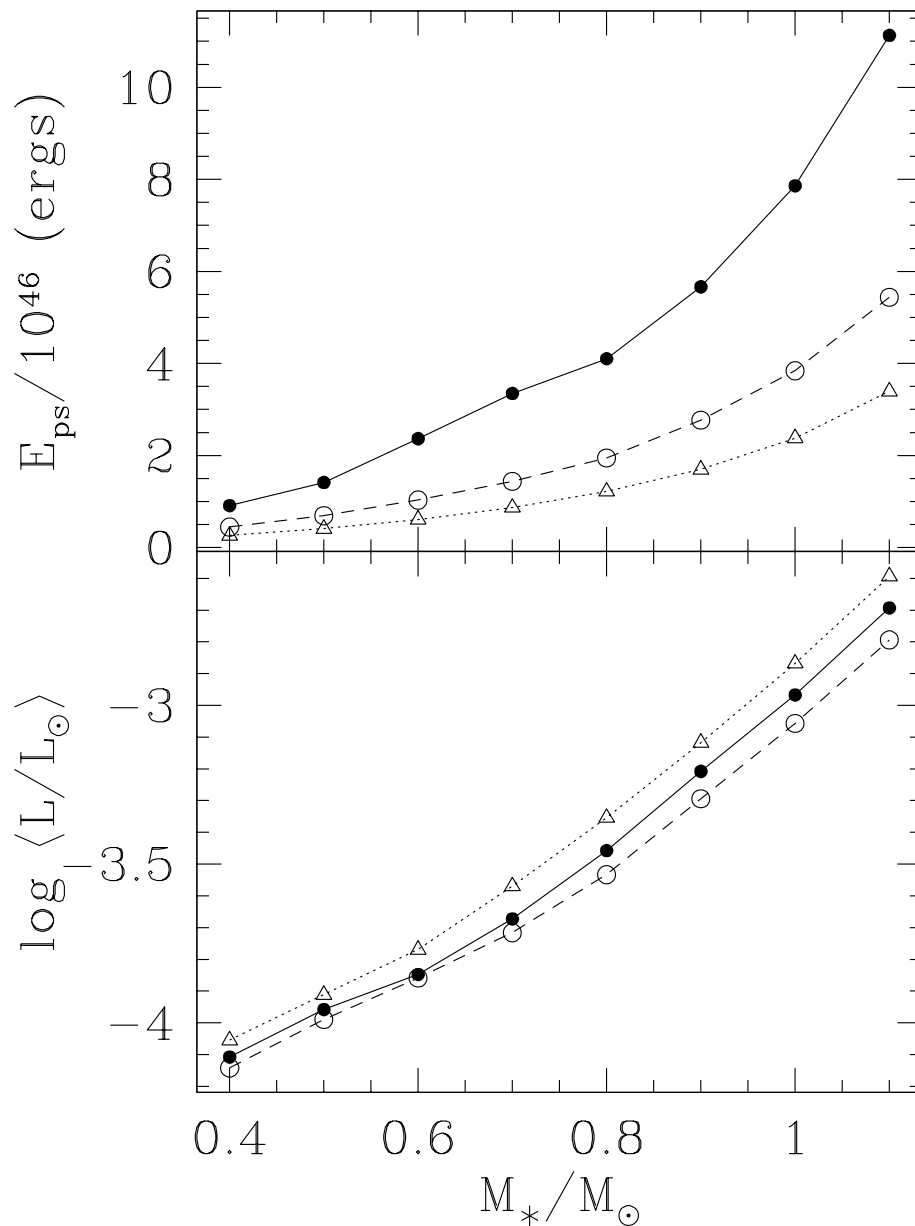


FIG. 7.— Phase separation energy and average luminosity as a function of mass, using the Segretain & Chabrier phase diagram. The solid curves are for initially homogeneous 50:50 C/O mixtures, the dashed curves are for the stratified C/O profile of Figure 4 (Salaris et al. 1997), and the dotted curves are for the stratified C/O profile of equation 7 (Wood 1995). The upper panel shows the total phase separation energy released as a function of total stellar mass, and the lower panel shows the average luminosity during the crystallization process, also as a function of total stellar mass.

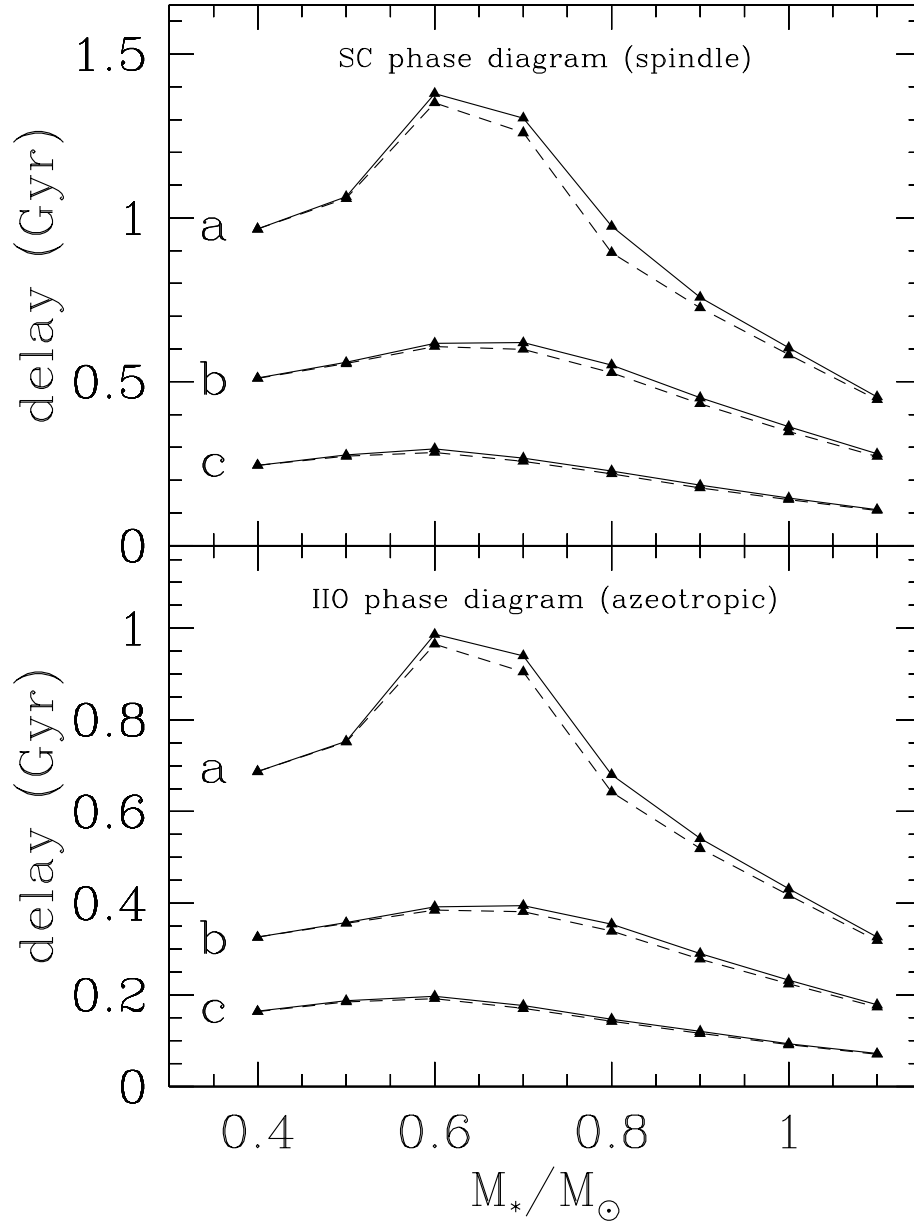


FIG. 8.— Age delay due to phase separation during crystallization as a function of total mass of the white dwarf model. Curve (a) corresponds to a 50:50 homogeneous initial C/O profile, while curves (b) and (c) are the initial profiles shown by the solid lines in Figures 4 and 3, respectively. The solid lines are for zero metallicity opacities and the dashed lines are for $Z = 0.001$, which shows that our result has little metallicity dependence. All models have $M_{\text{He}}/M_{\star} = 10^{-2}$ and $M_{\text{H}}/M_{\star} = 10^{-4}$.

age delays of 2–3 Gyr (Segretain et al. 1994; Hernanz et al. 1994). These species would arise from the initial abundance of metals in the main-sequence stars which later evolved into white dwarfs. This effect may only be important for Population I stars, however, and would not therefore affect the calculated ages of the cool white dwarfs which populate the turn-down in the WDLF, since these white dwarfs were formed very early in the history of the Galaxy (Hernanz et al. 1994).

In the context of Galactic evolution, age estimates for the oldest Galactic globular clusters range from 13–16 Gyr (Pont et al. 1998) to 11.5 ± 1.3 Gyr (Chaboyer et al. 1998), and depend on a variety of parameters. In addition, a 4 to 6 Gyr delay is expected between the formation of the globular clusters and that of the Galactic thin disk (e.g., Burkert, Truran, & Hensler 1992; Chiappini, Matteucci, & Gratton 1997), while the observed white dwarf luminosity function gives an age estimate for the thin disk of $9.5^{+1.1}_{-0.8}$ Gyr (Oswalt et al. 1996), without

including the effect of phase separation. Using the above numbers, we see that phase separation could add anywhere from 0 to 3 Gyr to the white dwarf ages and still be consistent with the overall picture of Galaxy formation. Our calculated maximum value of $\lesssim 1.5$ Gyr fits within these bounds, as does our best guess value of ~ 0.6 Gyr.

7. ACKNOWLEDGMENTS

We would like to thank M. Salaris for providing the oxygen profile shown in Figure 4, and we would like to thank the referee G. Chabrier for his valuable comments and suggestions.

This work was supported in part by the National Science Foundation under grant AST-9315461 (EWK, MHM, and DEW) and grant AST-9217988 (MAW) and by the NASA Astrophysics Theory Program under grant NAG5-2818 (EWK, MHM, and DEW) and grant NAG5-3103 (MAW).

REFERENCES

- Abrikosov, A. A. 1960, *Zh. Eksp. i Teor. Fiz.*, 39, 1798
 Barrat, J. L., Hansen, J. P., & Mochkovitch, R. 1988, *A&A*, 199, L15
 Bergeron, P., Wesemael, F., Lamontagne, R., Fontaine, G., Saffer, R. A., & Allard, N. F. 1995, *ApJ*, 449, 258
 Burkert, A., Truran, J. W., & Hensler, G. 1992, *ApJ*, 391, 651–658
 Chaboyer, B., Demarque, P., Kernan, P. J., & Krauss, L. M. 1998, *ApJ*, 494, 96
 Chabrier, G. 1998, In *Proceedings of IAU Symposium 189 on Fundamental Stellar Properties: The Interaction between Observation and Theory*, ed. T. R. Bedding, A. J. Booth, & J. Davis, volume 189 (Dordrecht: Kluwer), 381
 Chabrier, G., Segretain, L., Hernanz, M., Isern, J., & Mochkovitch, R. 1993, In *White Dwarfs: Advances in Observation and Theory*, ed. M. A. Barstow (Dordrecht: Kluwer Academic Publishers), 115
 Chandrasekhar, S. 1939, *An Introduction to the Study of Stellar Structure* (Chicago: University of Chicago Press)
 Chiappini, C., Matteucci, F., & Gratton, R. 1997, *ApJ*, 477, 765
 Clemens, J. C. 1993, PhD thesis, The University of Texas at Austin
 Clemens, J. C. 1995, *Baltic Astronomy*, 4, 142
 D’Antona, F. & Mazzitelli, I. 1978, *A&A*, 66, 453
 D’Antona, F. & Mazzitelli, I. 1989, *ApJ*, 347, 934
 DeWitt, H., Slattery, W., & Chabrier, G. 1996, *Physica B*, 228, 21
 García-Berro, E., Hernanz, M., Isern, J., Chabrier, G., Segretain, L., & Mochkovitch, R. 1996, *Astronomy and Astrophysics Supplement Series*, 117, 13
 García-Berro, E., Hernanz, M., Mochkovitch, R., & Isern, J. 1988, *A&A*, 193, 141
 Hernanz, M., García-Berro, E., Isern, J., Mochkovitch, R., Segretain, L., & Chabrier, G. 1994, *ApJ*, 434, 652
 Ichimaru, S., Iyetomi, H., & Ogata, S. 1988, *ApJ*, 334, L17
 Iglesias, C. A. & Rogers, F. J. 1993, *ApJ*, 412, 752
 Isern, J., Mochkovitch, R., García-Berro, E., & Hernanz, M. 1997, *ApJ*, 485, 308
 Kirzhnits, D. A. 1960, *Soviet Phys.—JETP*, 11, 365
 Lamb, D. Q. & Van Horn, H. M. 1975, *ApJ*, 200, 306
 Lamontagne, R., Wesemael, G., Fontaine, G., & Demers, S. 1997, In *White Dwarfs, Proceedings of the 10th European Workshop on White Dwarfs*, ed. J. Isern, M. Hernanz, & E. García-Berro (Dordrecht, Boston, London: Kluwer Academic Publishers), 143
 Liebert, J., Dahn, C. C., & Monet, D. G. 1988, *ApJ*, 332, 891
 Mazzitelli, I. & D’Antona, F. 1986, *ApJ*, 308, 706
 Mestel, L. 1952, *MNRAS*, 112, 583
 Mestel, L. & Ruderman, M. A. 1967, *MNRAS*, 136, 27
 Mochkovitch, R. 1983, *A&A*, 122, 212
 Ogata, S. & Ichimaru, S. 1987, *Phys. Rev. A*, 42, 5451
 Oswalt, T. D., Smith, J. A., Wood, M. A., & Hintzen, P. 1996, *Nature*, 382, 692
 Pont, F., Mayor, M., Turon, C., & Vandenberg, D. A. 1998, *A&A*, 329, 87
 Salaris, M., Dominguez, I., García-Berro, E., Hernanz, M., Isern, J., & Mochkovitch, R. 1997, *ApJ*, 486, 413
 Salpeter, E. 1961, *ApJ*, 134, 669
 Schmidt, M. 1959, *ApJ*, 129, 243
 Schwarzschild, K. 1958, *Structure and Evolution of the Stars* (Princeton: Princeton University Press)
 Segretain, L. & Chabrier, G. 1993, *A&A*, 271, L13
 Segretain, L., Chabrier, G., Hernanz, M., García-Berro, E., Isern, J., & Mochkovitch, R. 1994, *ApJ*, 434, 641
 Stevenson, D. J. 1977, *Proc. Ast. Soc. Australia*, 3, 167
 Stevenson, D. J. 1980, *J. Phys. Suppl.*, 41, C2–61
 Van Horn, H. M. 1968, *ApJ*, 151, 227
 Weidemann, V. & Koester, D. 1983, *A&A*, 121, 77
 Weidemann, V. & Yuan, J. W. 1989, In *White dwarfs: Proceedings of IAU Colloquium 114th, Hanover, NH*, ed. G. Wegner (Berlin, New York: Springer-Verlag), 1
 Winget, D. E., Hansen, C. J., Liebert, J., Van Horn, H. M., Fontaine, G., Nather, R. E., Kepler, S. O., & Lamb, D. Q. 1987, *ApJ*, 315, L77
 Wood, M. 1993, *Bull. American Astron. Soc.*, 183, 5002
 Wood, M. 1995, In *White Dwarfs: Proceedings of the 9th European Workshop on White Dwarfs*, ed. D. Koester & K. Werner (Berlin, Heidelberg: Springer-Verlag), 41
 Wood, M. A. 1990, PhD thesis, The University of Texas at Austin
 Wood, M. A. 1992, *ApJ*, 386, 539–561
 Wood, M. A. & Oswalt, T. D. 1998, *ApJ*, 497, 870
 Wood, M. A. & Winget, D. E. 1989, In *White dwarfs: Proceedings of IAU Colloquium 114th, Hanover, NH*, ed. G. Wegner (Berlin, New York: Springer-Verlag), 282
 Xu, Z. W. & Van Horn, H. M. 1992, *ApJ*, 387, 662